Res Chem Intermed (2015) 41:2095–2124
DOI 10.1007/s11164-013-1334-6

DFT studies on the stability of linear, ring, and 3D structures in CdTe nanoclusters

S. Sriram · R. Chandiramouli

Received: 25 December 2012 / Accepted: 4 July 2013 / Published online: 30 August 2013

Abstract In DFT studies with the B3LYP/LanL2DZ basis set the different structures, linear, ring, and 3D, of cadmium telluride $(CdTe)_n$ clusters for $n = 2$–7 were completely optimized. The stability, dipole moment, and point groups of the different clusters were studied. The HOMO–LUMO energy gap, ionization potential, electron affinity, relative stability, and binding energy of different clusters were studied and compared with values for different isomers. These results for the different properties of CdTe nanoclusters will give clear information enabling the design of new materials with potential importance in thin-film solar cells.

Keywords Nanocluster · Stability factor · Binding energy · DFT · B3LYP · LanL2DZ

Introduction

Cadmium telluride (CdTe), a group II–VI compound semiconductor has a narrow direct optical band gap of approximately 1.5 eV [1, 2]. CdTe has a lattice constant of 0.648 nm at room temperature. CdTe is usually transparent in the infrared region but is fluorescent at 790 nm. When the size of CdTe is reduced and electron movement is confined, producing CdTe quantum dots, the peak of fluorescence may shift toward the UV–visible region. CdTe has an absorption coefficient $>5 \times 10^5$/cm. Because of the narrow band gap and high absorption coefficient, approximately $\sim$99 % of photons which have energy greater than the

S. Sriram · R. Chandiramouli (✉)
School of Electrical & Electronics Engineering, SASTRA University, Tirumalaisamudram, Thanjavur 613401, India
e-mail: rcmoulii@gmail.com

bandgap will be absorbed by CdTe films, which are, therefore, promising materials for thin-film solar cells [3–5]. CdTe is appropriate for nano-structured thin films which can overcome the short diffusion length of minority charge carriers. CdTe modules are used for high-energy performance and attract large-scale capital investment. Major applications of CdTe include infrared optical windows [6], infrared detectors (HgCdTe) [7, 8], X-ray and gamma ray detectors (CdZnTe) [9, 10], and electro-optic modulators [11]. An important advantage of CdTe is the flexibility of the method of manufacture. CdTe thin films can be synthesized by such methods as sputtering [12, 13], electrodeposition [14, 15], spraying [16], pulse laser deposition [17, 18], and chemical vapour deposition [19].

This work was performed to study the stability of CdTe nanoclusters, and some of their physical properties, for possible application in nanotechnology-based solar cells. During synthesis, if growth of the clusters is restricted in different ways, by growing the cluster in an orientated substrate or by capping CdTe with a surfactant, clusters will be formed with a particular orientation. The geometry of the cluster can be finely adjusted to improve structural stability and electronic properties; this motivated investigation of different, realistic, structures of CdTe nanoclusters. A literature survey revealed little work has been conducted on CdTe nanoclusters. Nanocage and multicage structures have been reported [20–22].

Density functional theory (DFT) is a good method for study of the electronic properties of CdTe clusters. Although experimental work has been performed to study their structure and electronic properties, it is still difficult to obtain information about the electronic properties of CdTe quantum dots by use of experimental methods. Fine adjustment of the structure of CdTe during synthesis to furnish different structures, namely linear, ring and 3D structures are reported in the present work.

Computational methods

Structures of $(CdTe)_n$ for $n = 2$–7 nanoclusters were completely optimized by use of the Gaussian 03 W package [23]. Quantum chemical calculation for $(CdTe)_n$ was performed by use of the DFT technique with Beckee's three-parameter hybrid functions in combination with the Lee–Yang–Parr correlation functional method (B3LYP) with the LanL2DZ basis set [24–27]. In quantum mechanical calculations the pseudo potential approximation is used to replace the complex effects of motion of electrons bound to an atom. The effective potential of the nucleus is referred as the pseudo potential because the Schrödinger equation contains a modified potential term. Because the atomic numbers of cadmium and tellurium are 48 and 52, respectively, the complete LanL2DZ basis set, which is applicable to the elements H, Li–La, and Hf–Bi, gives the best results with the pseudo potential approximation. The B3LYP/LanL2DZ basis set is thus suitable for complete optimization of the structures of $(CdTe)_n$ clusters. HOMO–LUMO gaps and density of states (DOS) were calculated from Gaussian output by use of the Gauss Sum 2.2 package [28].

Results and discussion

Structures of $(CdTe)_n$

The structures of $(CdTe)_n$ for $n = 1$–7 are depicted in Figs. 1, 2, and 3 for linear, ring, and 3D structures respectively. For linear structures of CdTe, addition of atoms to the cluster leads to increased stability; the increase in stability is linear and the difference between two successive clusters is 56 Hartrees. For ring structures, also, the stability increases with increasing number of atoms. Because the ring structure is a closed structure, comparing the energy of the ring structure with that of the linear structure results in a slight increase in the stability of the fractional part only. The same trend in increased stability is seen for the 3D structure, which is more stable than the ring structures. Although the ring structure is a two-dimensional structure, stability is greater for ring structures with $n = 3$, 5, and 7 than for 3D clusters, possibly because of the formation of a closed loop of atoms in the cluster. Among the three different structures, the $(CdTe)_7$ ring structure has the minimum energy and the atoms in that structure are equally placed at distances of approximately 2.8 Å. In general, for all the clusters the bond lengths were optimized at almost 2.8 Å, in good agreement with the bond length of bulk CdTe.

Dipole moments are greater for the linear structure than for the other two structures, because in the linear structure the atoms are aligned in straight line and are truncated at the ends. Maximum values of 8.422 and 8.196 Debye are observed for the linear structure of $(CdTe)_5$ and the 3D structure of $(CdTe)_7$, respectively. The dipole moments arise because of difference between the centre of charges. Because the electronic configuration varies depending on cluster size, there is a zigzag variation in the dipole moment of linear, ring, and 3D structures. The dipole moments of all the ring structures are lowest because the ring structures are closed loop structures. The lowest dipole moment, approximately 0.0214 Debye, is observed for the $(CdTe)_2$ ring structure. It was also found that, irrespective of structure, if the dipole moment was lowest for a particular cluster the energy also was lowest, and that stability increased with cluster size. The ring structure has point symmetry of C_1 for all the clusters. However, for both linear and 3D structures point symmetry of C_1, C_S, C_{2V}, and $C_{\infty V}$ are observed, i.e. asymmetry is high for all the structures. Energy, dipole moment, and point symmetry of $(CdTe)_n$ for $n = 2$–7 are shown in Table 1. From the results it can be inferred that the stability of the clusters will depend on the cluster size only, not on the different structures linear, ring, or 3D. The variation in the energy is only in the fractional part. For fewer atoms in the cluster, the cluster is in the premature state and addition of atoms to the cluster increases its stability.

HOMO–LUMO energies of $(CdTe)_n (n = 2$–$7)$

The HOMO–LUMO energy gaps of $(CdTe)_n$ ($n = 2$–7) are illustrated in Table 2. It is observed that the calculated values of the energy gaps indicate that all the clusters are semiconductors. Interestingly, the HOMO–LUMO gap decreases with increasing cluster size, i.e. with increasing number of atoms in the cluster, because the band

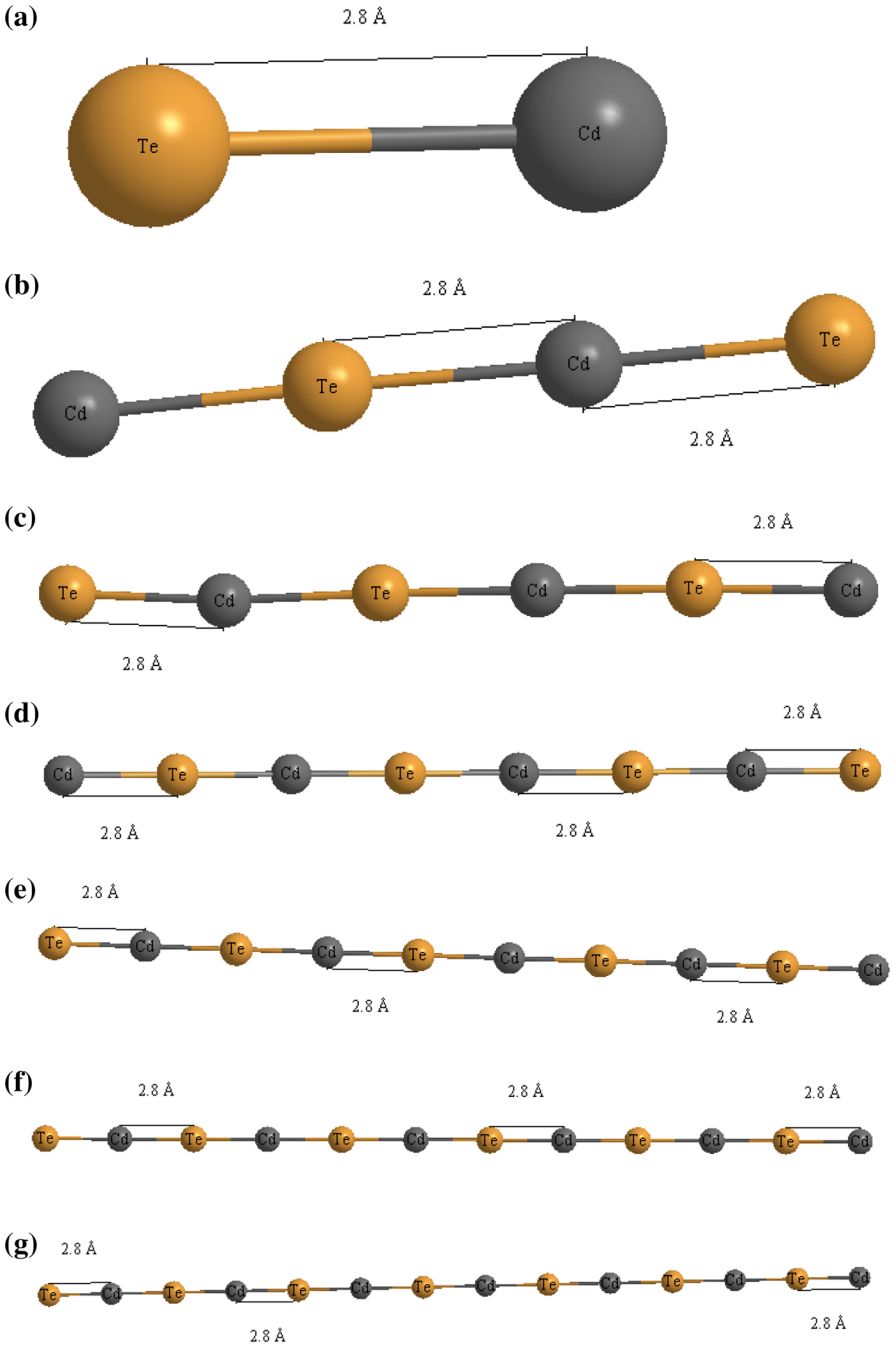

Fig. 1 **a–g** B3LYP/LanL2DZ optimized linear structures of $(CdTe)_n$ ($n = 1–7$)

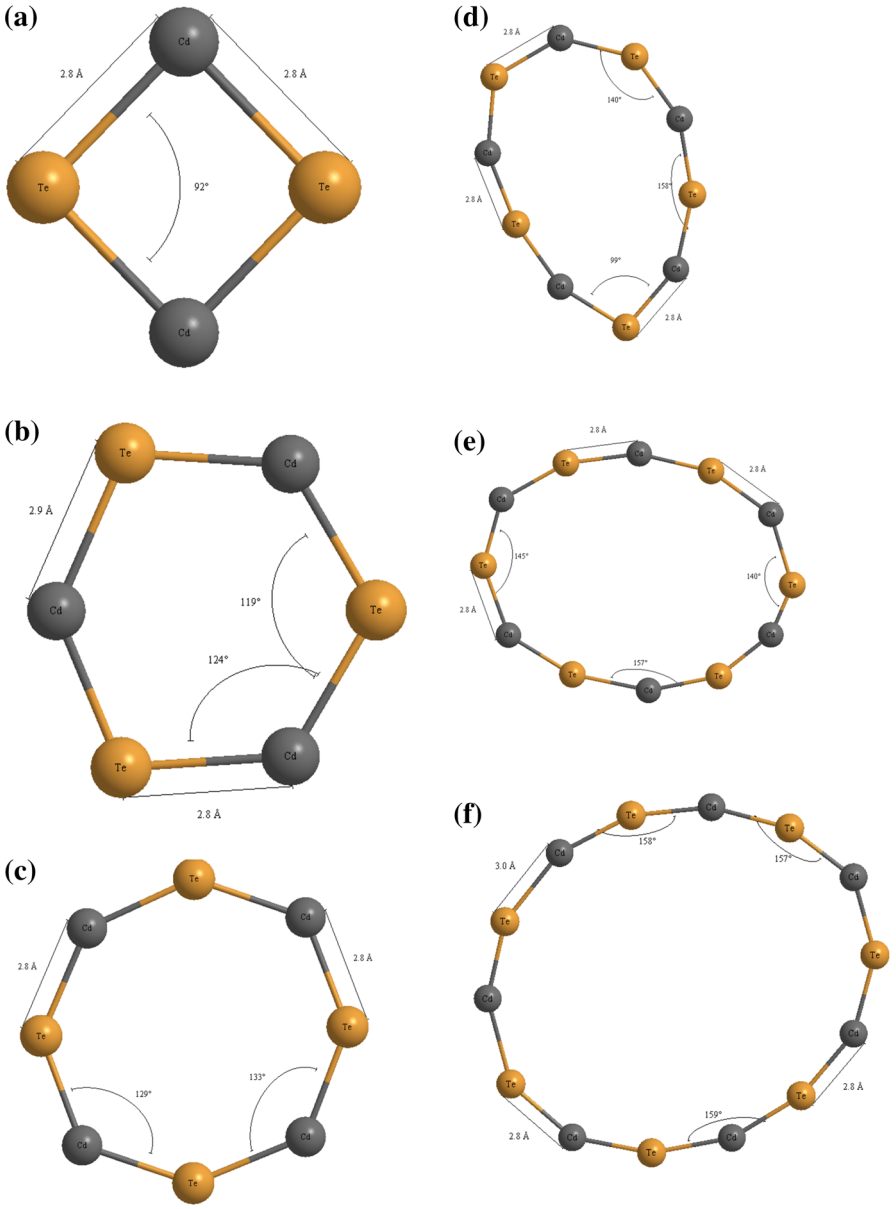

Fig. 2 **a–f** B3LYP/LanL2DZ optimized ring structures of $(CdTe)_n$ ($n = 2$–7)

gap decreases with overlapping of the orbitals. Overlap of the *s* and *d* orbitals of the Cd atom with the *p* orbital of Te atom leads to a surface passivation effect which in turn reduces the HOMO–LUMO gap when cluster size increases. Clusters with large HOMO–LUMO gaps are chemically inert because it is unfavourable to add electrons to a high-lying LUMO level or to remove electrons from a low-lying

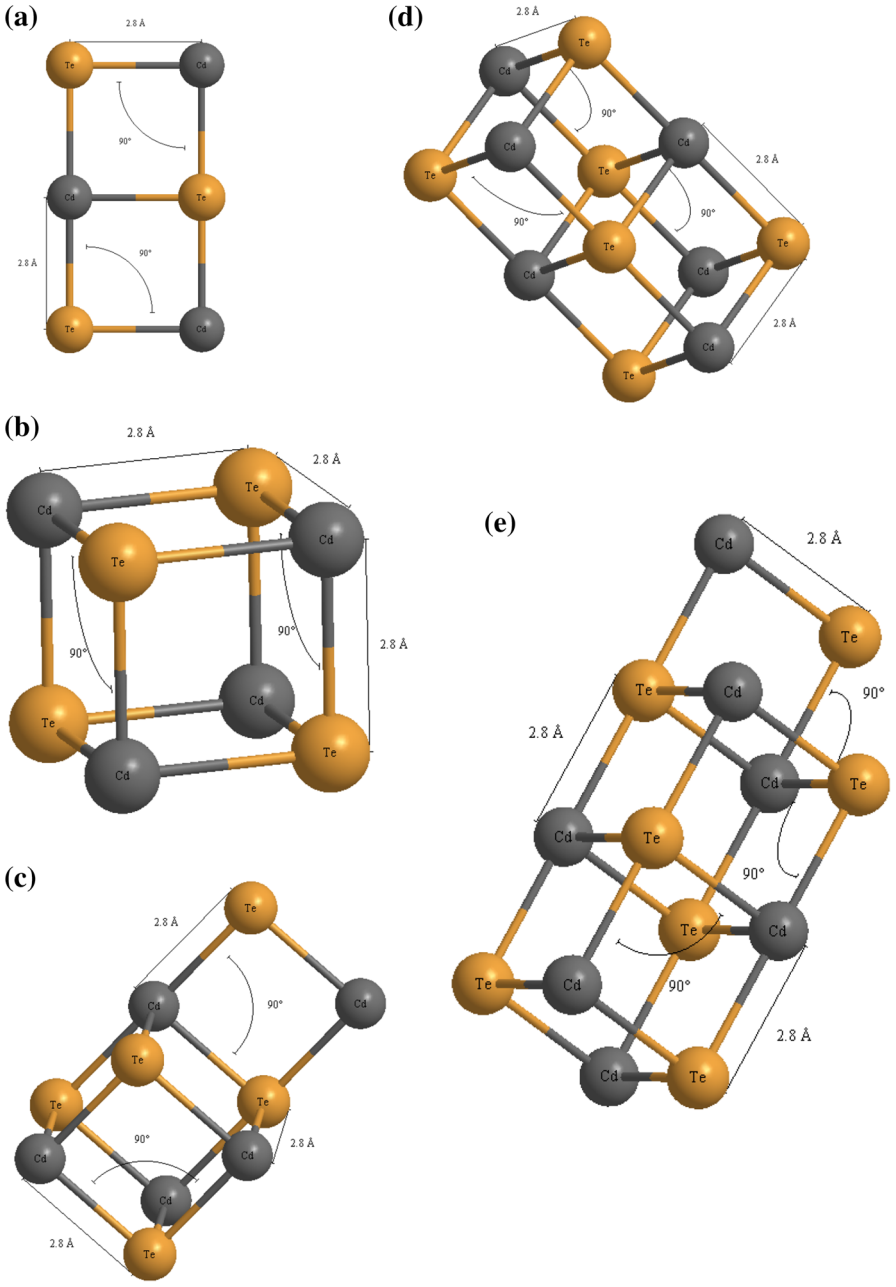

Fig. 3 **a–e** B3LYP/LanL2DZ optimized 3D structures of $(CdTe)_n$ ($n = 3$–7)

HOMO level [29, 30]. The decrease in the HOMO–LUMO gap is almost linear for linear structures of $(CdTe)_n$. The calculated maximum HOMO–LUMO gap for the linear structure is observed for $n = 1$ which has an energy gap of 1.06 eV; this can,

Table 1 Energy and dipole moment of $(CdTe)_n$ ($n = 2$–7) clusters

Structure	Cluster size	Energy (Hartrees)	Dipole moment (Debye)	Point group
Linear	1	−56.102	5.3864	$C_{\infty V}$
	2	–112.239	5.5919	C_1
	3	–168.39	6.3951	C_1
	4	–224.54	7.6247	C_S
	5	–280.689	8.4222	C_S
	6	–336.837	1.7188	C_S
	7	–392.983	1.4752	C_S
Ring	2	–112.263	0.0214	C_1
	3	–168.483	0.1941	C_1
	4	–224.602	0.3882	C_1
	5	–280.803	1.2284	C_1
	6	–336.746	1.3117	C_1
	7	–393.042	2.1587	C_1
3D	3	–168.47	5.8332	C_{2V}
	4	–224.622	0.0422	C_1
	5	–280.78	5.1625	C_1
	6	–336.981	0.0966	C_S
	7	–381.229	8.1967	C_1

therefore, be regarded as a building block for this kind of linear structure. For ring structures, however, the gap increases and decreases depending on the placement of atoms in the structure. The minimum and maximum values of the calculated energy gap for the CdTe ring structure are 0.52 and 1.35 eV for $n = 7$ and $n = 3$ respectively. The HOMO–LUMO gap is appreciable for 3D structures. It is almost constant for these structures except for $n = 7$, possibly because of the formation of ladder-like structures with more atoms in the structure. Overlap of the Cd *s* orbital and Te *p* orbital for greater numbers of atoms may result in the consistent HOMO–LUMO energy gap in the 3D structures. Because of the arrangements of the atoms in all three types of CdTe cluster, the band gaps of the linear $n = 1$, ring $n = 5$, and 3D $n = 5$ clusters are similar, $\sim$1.06 eV, possibly because of the similar arrangements of atoms in these three different clusters. HOMO–LUMO gaps and DOS for $(CdTe)_n$ ($n = 2$–7) are listed in Table 3. The range of DOS values provides insight to the density of the charge along the Fermi level. For linear CdTe nanoclusters the density of the charge is nearer the Fermi level in the occupied orbital. Location of charge near a Fermi level with a small HOMO–LUMO gap will enable easier movement of electrons to the virtual orbital. Study of the ring structures of CdTe clusters reveals greater location of charge near the Fermi level; it should also be noted that more states are seen in the virtual orbital. This may be because formation of the closed loop in ring structure gives rise to the localization of charge in the virtual orbital. Interestingly, the density of charges in the 3D structures is distant from the Fermi level, because of formation of clusters of the atoms in three dimensions. For the 3D structure with $n = 7$ there is wide gap with

maximum density of charge distant from occupied and virtual orbitals. The HOMO–LUMO gaps of CdTe nanoclusters are in good agreement with reported results [31].

Ionization potential, electron affinity, and relative stability of CdTe nanoclusters

IP and EA provide fundamental insight to the electronic structure of the nanoclusters. For the linear structure the ionization potential is almost constant, approximately 5.7 eV, with little variation. This may be because linear alignment of the atoms results in little change in the electronic configuration. The electron affinity increases with increasing cluster size and may reach saturation for higher-order clusters. The trend in the ionization potential for the ring structure of $(CdTe)_n$ seems to be a zigzag path; removal of electrons from the clusters will depend on the positions of the atoms in the ring structure [32]. Electron affinity also varies randomly with cluster size. The ionization potential for 3D structures is almost the same up to $n = 6$ then increases for $n = 7$, implying that $(CdTe)_7$ is more chemically reactive than the other CdTe clusters. Remarkably, the electron affinity for the $n = 7$ 3D cluster is less than that of the other clusters. Figure 4a–c depicts IP and EA variation with cluster size for $(CdTe)_n$ ($n = 2$–7) with linear, ring and 3D clusters, respectively.

Another important property used as an indicator of the stability of geometrically optimized CdTe clusters is the relative stability ($\Delta_2(n)$), which can be calculated by use of the equation:

Table 2 HOMO–LUMO energies of $(CdTe)_n$ ($n = 2$–7) clusters

Structure	Cluster size	HOMO (eV)	LUMO (eV)	Energy gap (eV)
Linear	1	−5.45	−4.39	1.06
	2	−5.72	−5.23	0.49
	3	−5.79	−5.46	0.33
	4	−5.79	−5.54	0.25
	5	−5.77	−5.58	0.19
	6	−5.75	−5.6	0.15
	7	−5.77	−5.69	0.08
Ring	2	−4.85	−4.3	0.55
	3	−5.52	−4.17	1.35
	4	−5.39	−4.65	0.74
	5	−5.52	−4.46	1.06
	6	−5.44	−4.86	0.58
	7	−5.56	−5.04	0.52
3D	3	−5.53	−3.85	1.68
	4	−5.23	−4.01	1.22
	5	−5.1	−3.97	1.13
	6	–4.92	–3.67	1.25
	7	–6.58	–1.59	4.99

Table 3 HOMO–LUMO, DOS diagrams of $(CdTe)_n$ ($n = 2$–7) clusters

No.	Structure	Cluster size	HOMO–LUMO, DOS
1	Linear	1	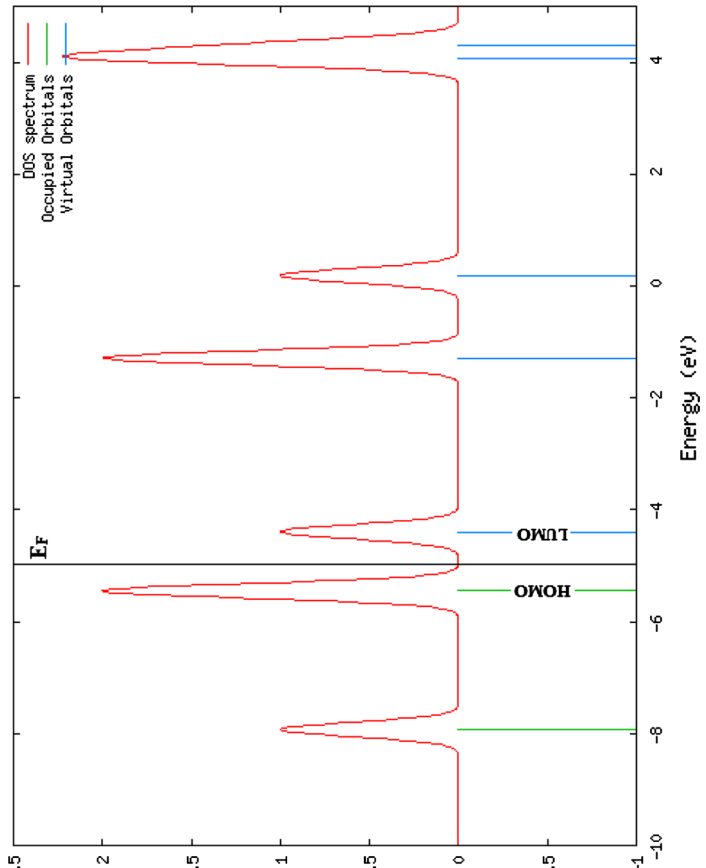

Table 3 continued

No.	Structure	Cluster size	HOMO–LUMO, DOS
2		2	

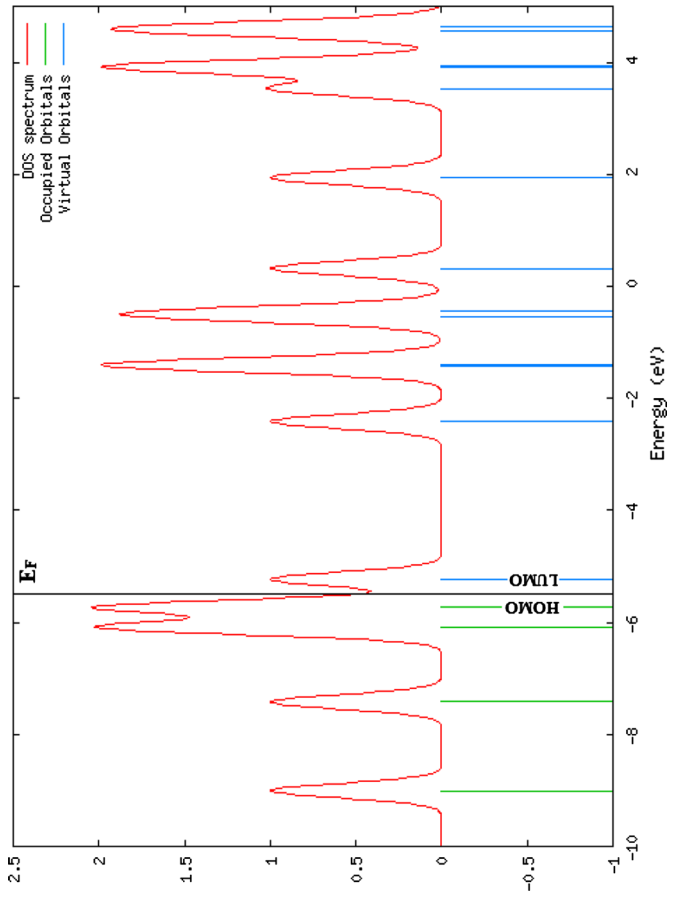

Table 3 continued

No.	Structure	Cluster size	HOMO–LUMO, DOS
3		3	

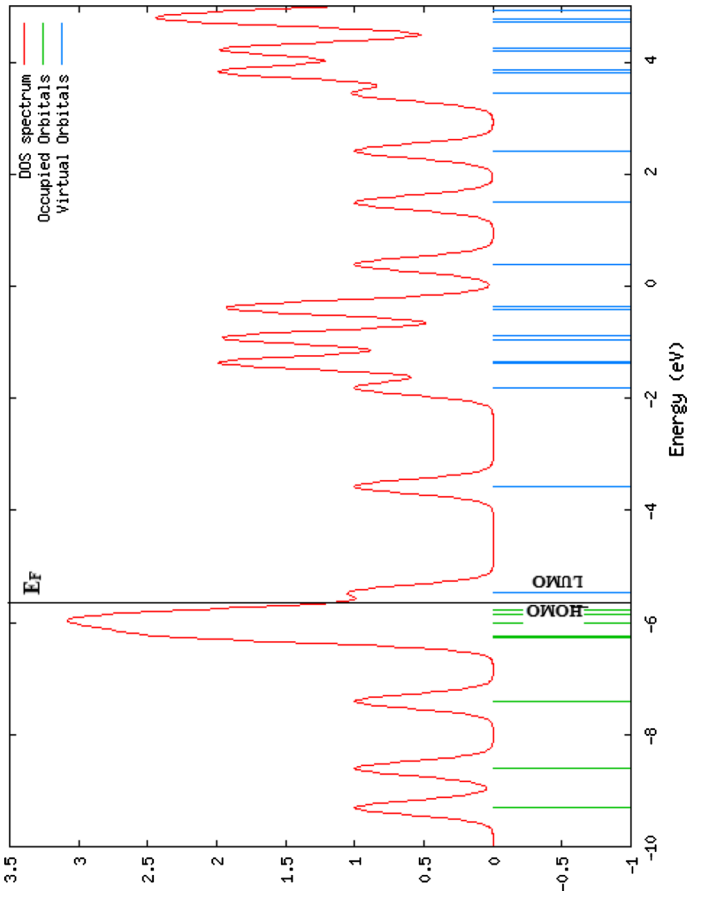

Table 3 continued

No.	Structure	Cluster size	HOMO–LUMO, DOS
4		4	

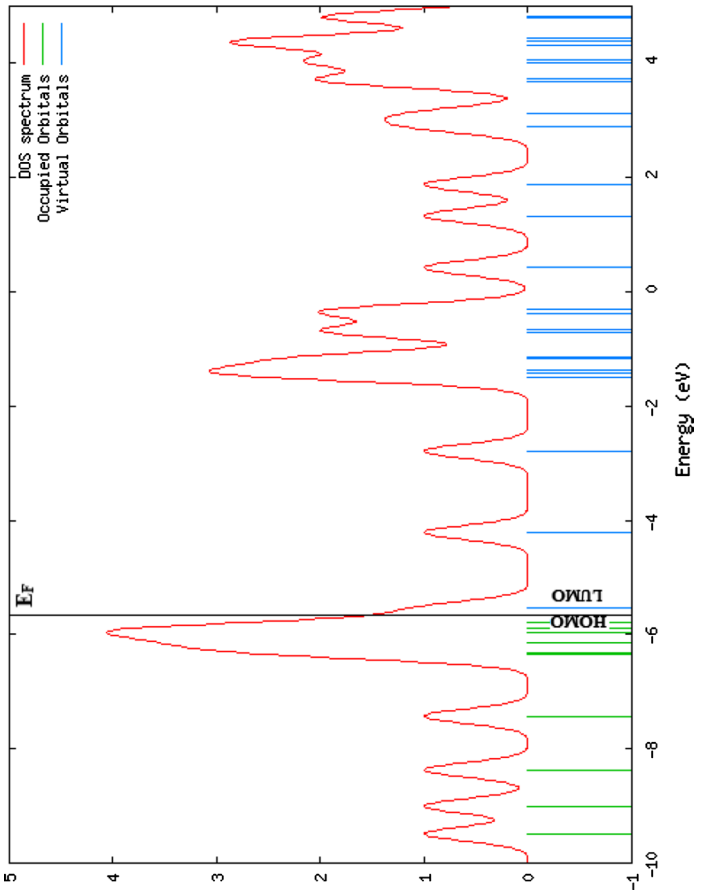

Table 3 continued

No.	Structure	Cluster size	HOMO–LUMO, DOS
5		5	

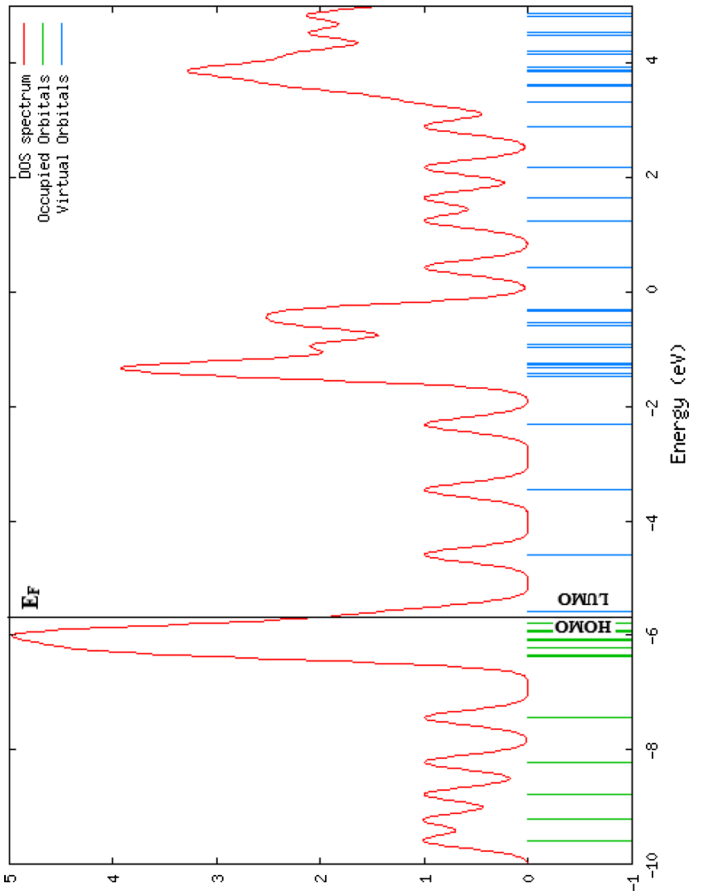

Table 3 continued

No.	Structure	Cluster size	HOMO–LUMO, DOS
6		6	

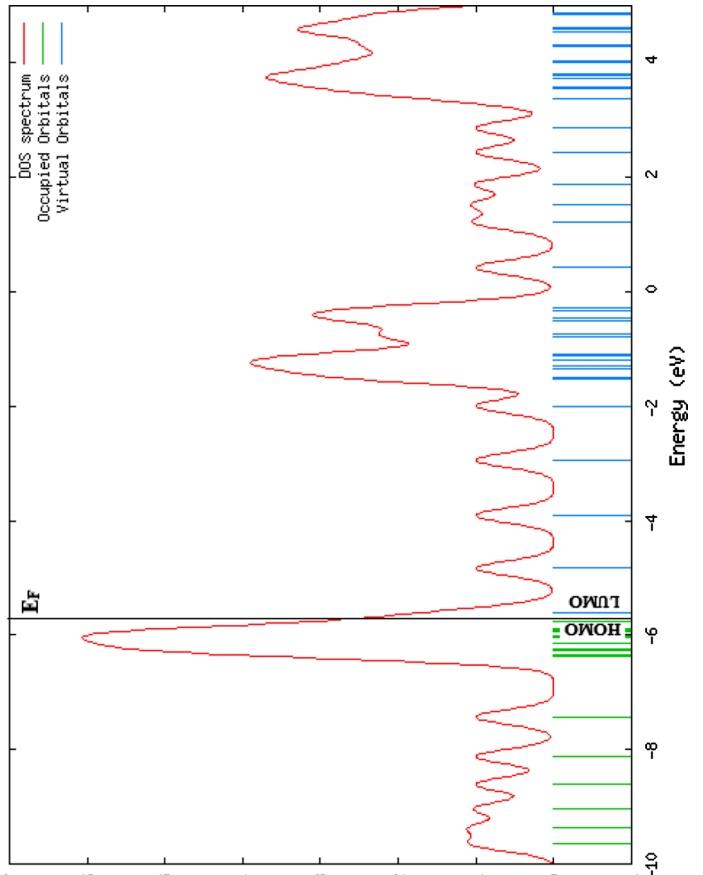

Table 3 continued

No.	Structure	Cluster size	HOMO–LUMO, DOS
7		7	

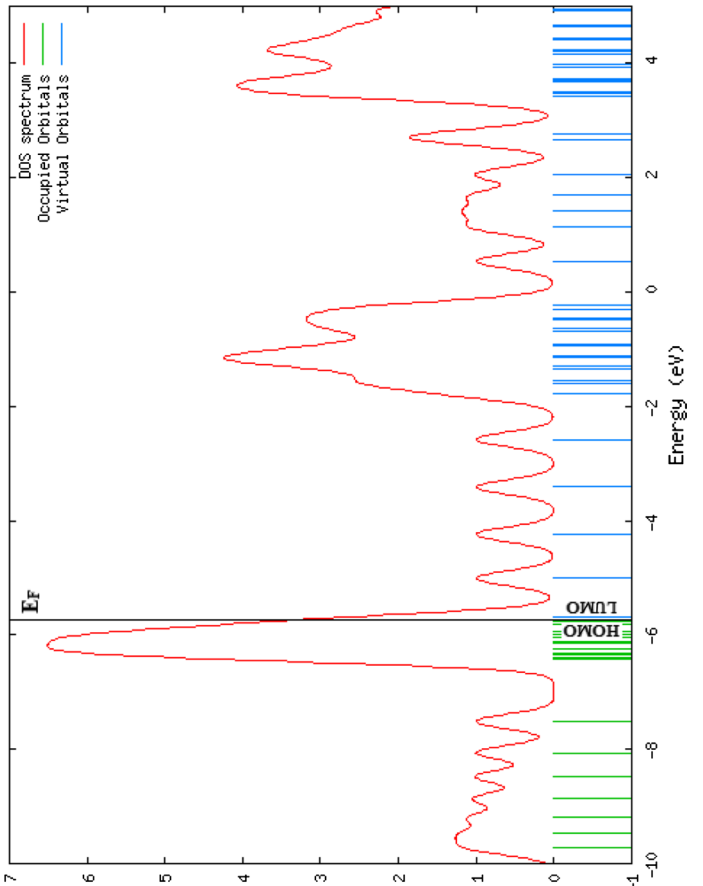

Table 3 continued

No.	Structure	Cluster size	HOMO–LUMO, DOS
8	Ring	2	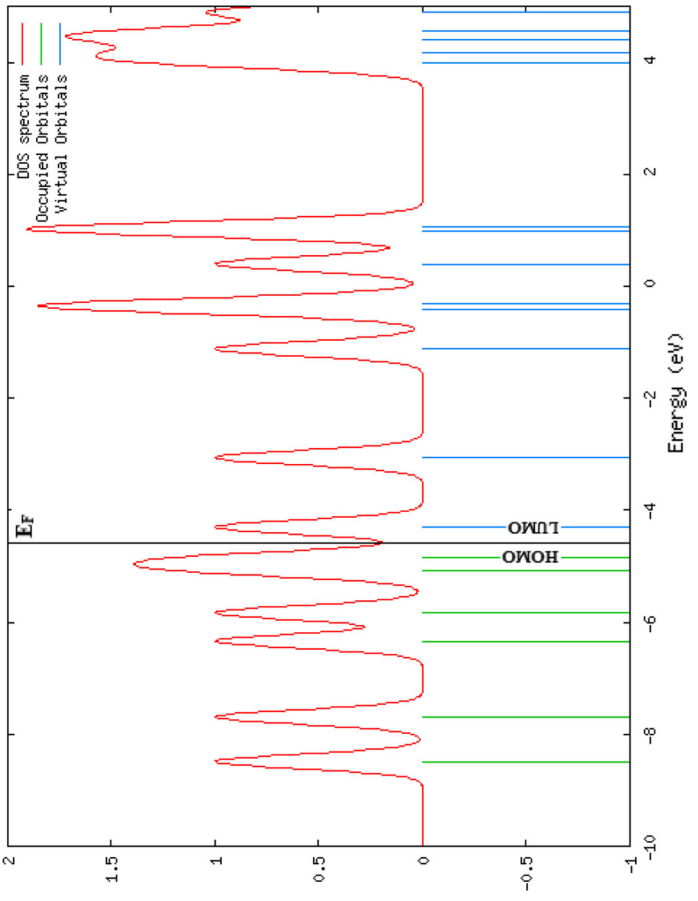

Table 3 continued

No.	Structure	Cluster size	HOMO–LUMO, DOS
9		3	

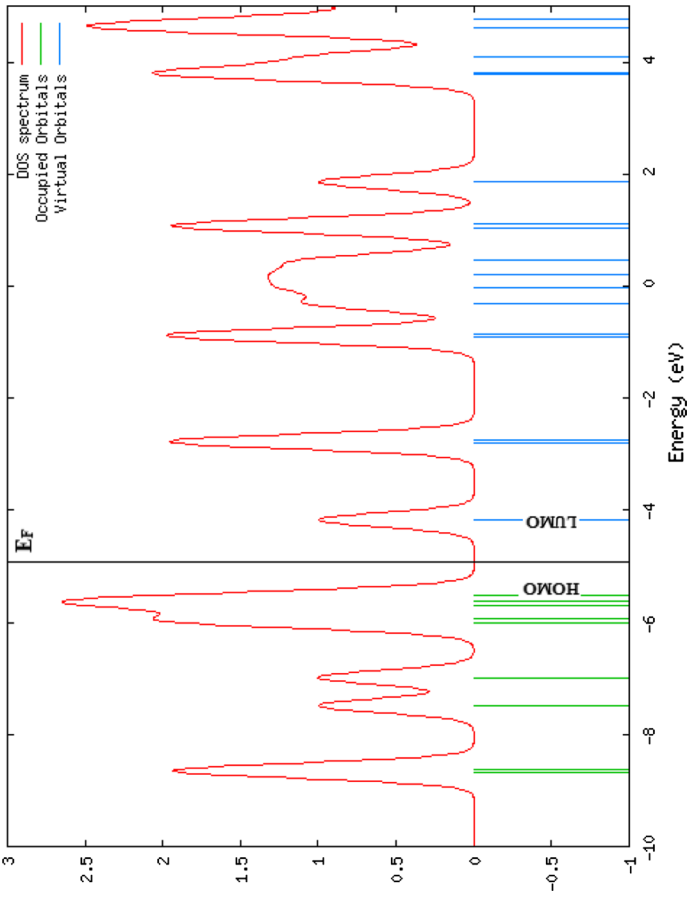

Table 3 continued

No.	Structure	Cluster size	HOMO–LUMO, DOS
10		4	

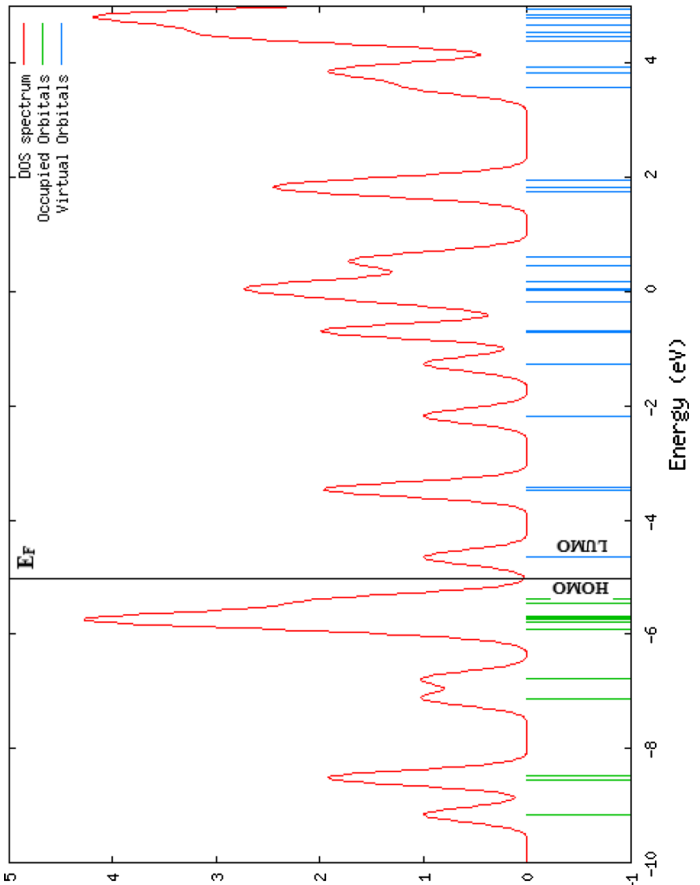

Table 3 continued

No.	Structure	Cluster size	HOMO–LUMO, DOS
11		5	

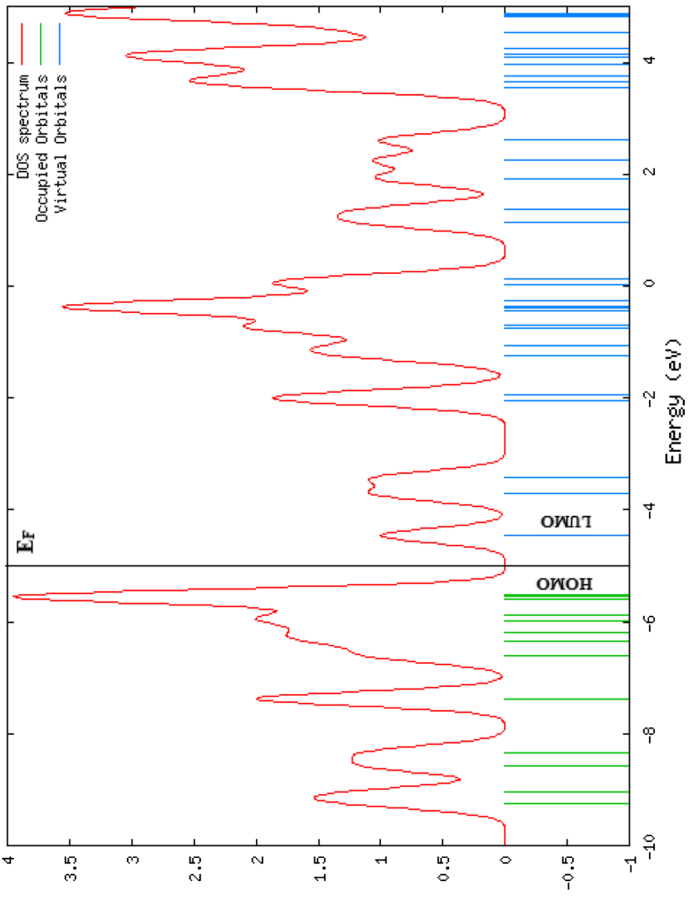

Table 3 continued

No.	Structure	Cluster size	HOMO–LUMO, DOS
12		6	

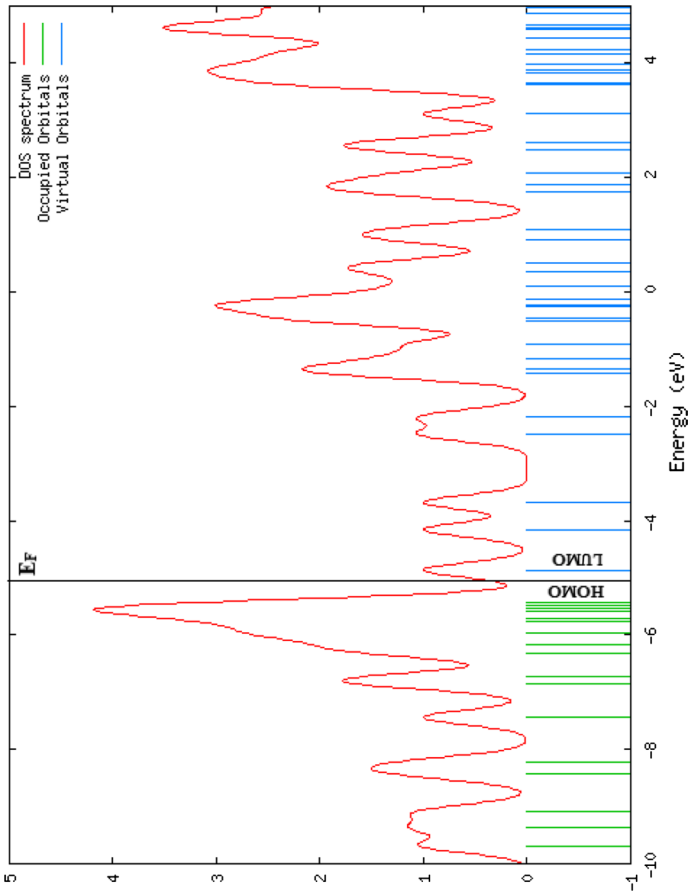

Table 3 continued

No.	Structure	Cluster size	HOMO–LUMO, DOS
13		7	

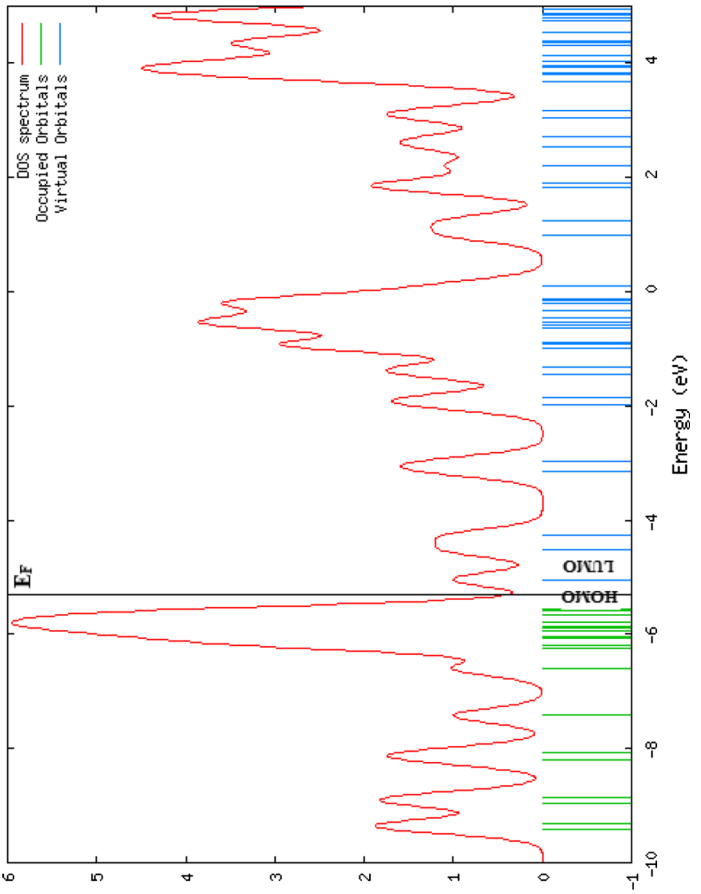

Table 3 continued

No.	Structure	Cluster size	HOMO–LUMO, DOS
14	3D	3	

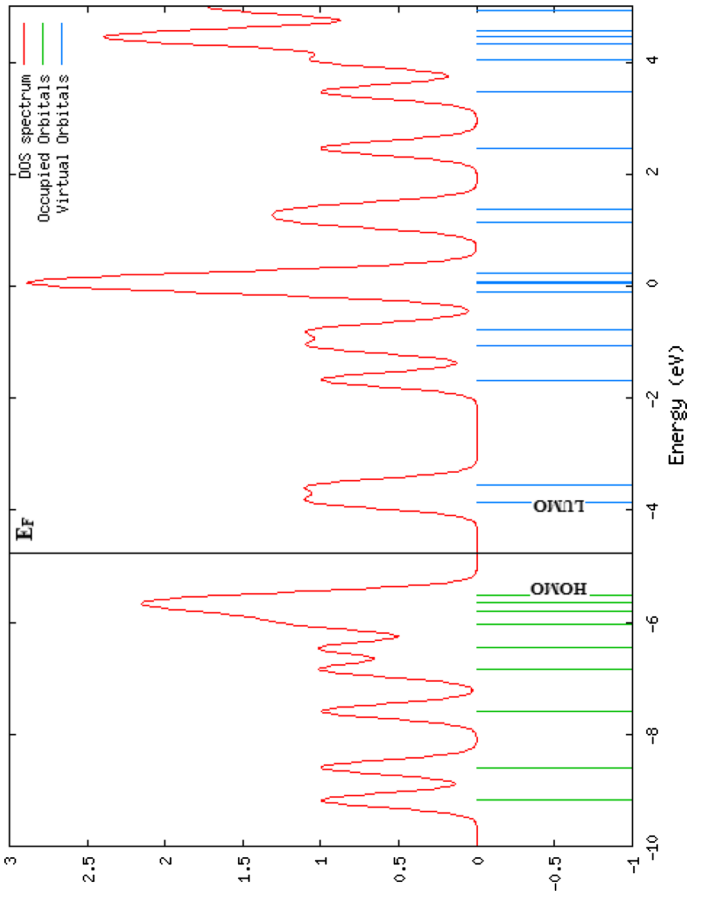

Table 3 continued

No.	Structure	Cluster size	HOMO–LUMO, DOS
15		4	

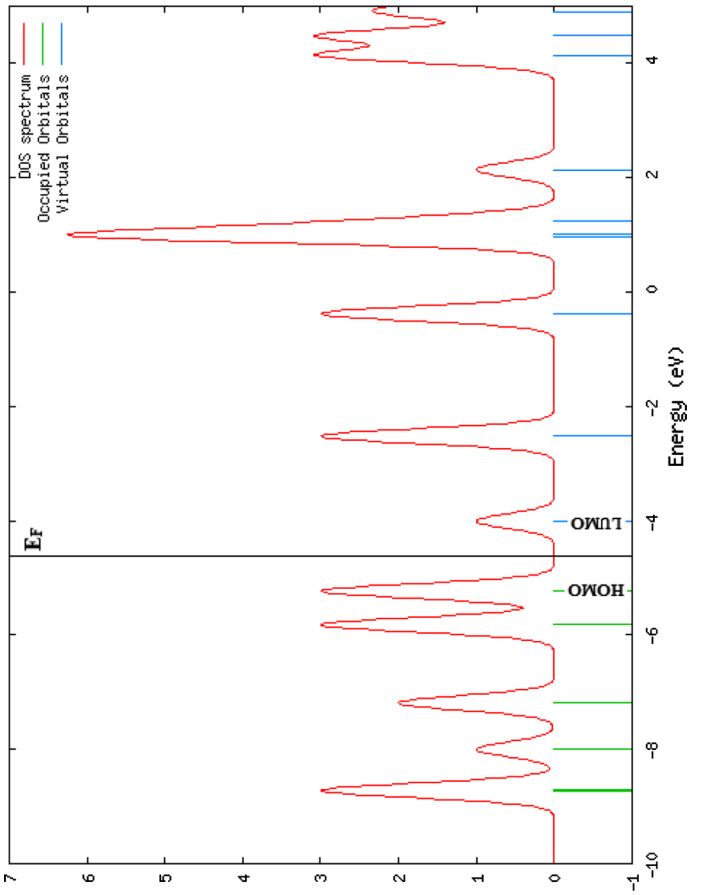

Table 3 continued

No.	Structure	Cluster size	HOMO–LUMO, DOS
16		5	

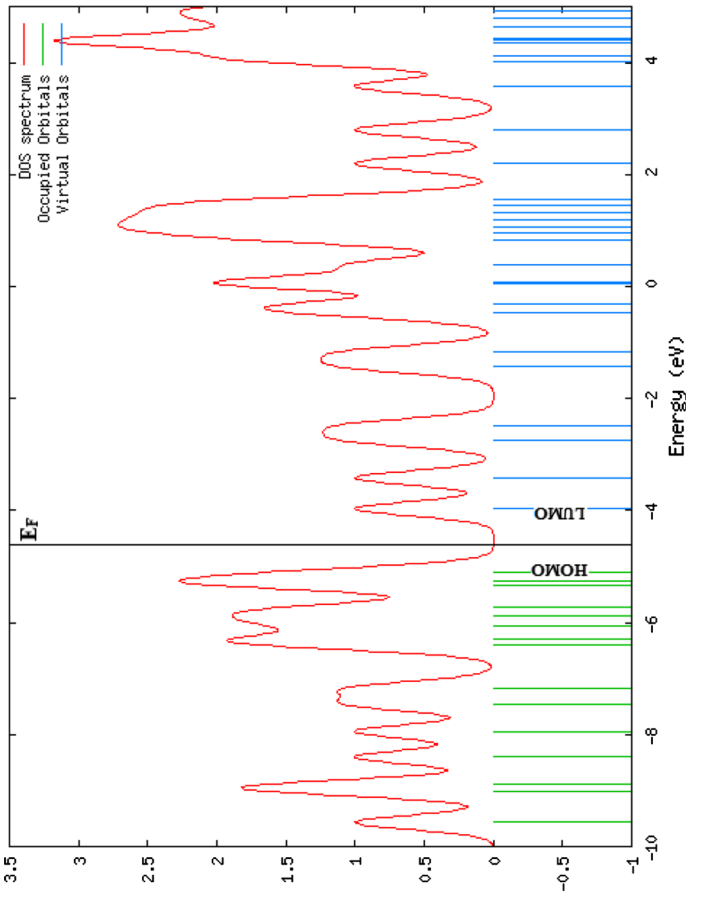

Table 3 continued

No.	Structure	Cluster size	HOMO–LUMO, DOS
17		6	

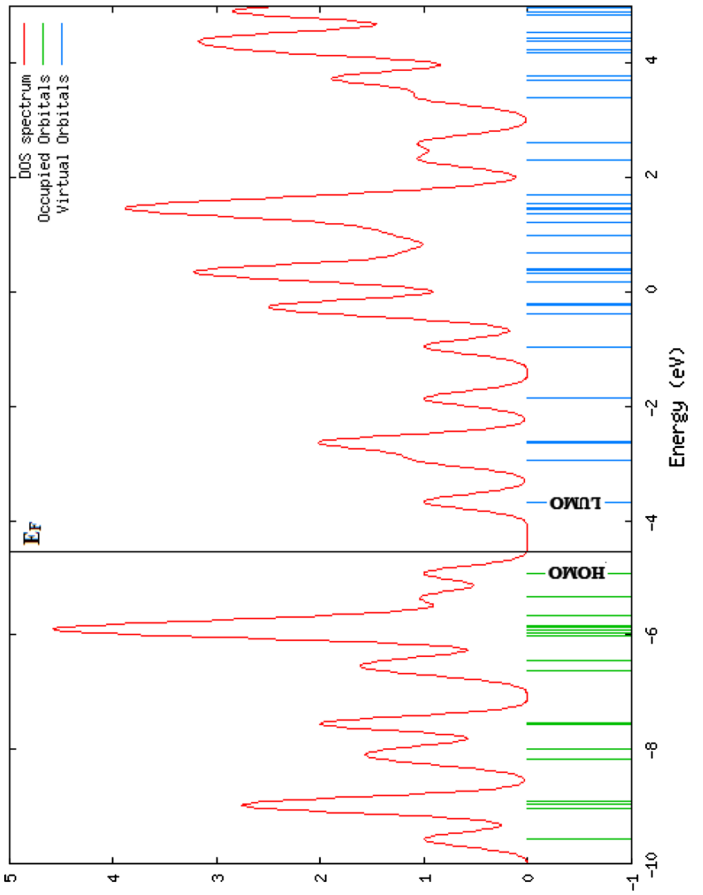

Table 3 continued

No.	Structure	Cluster size	HOMO–LUMO, DOS
18		7	

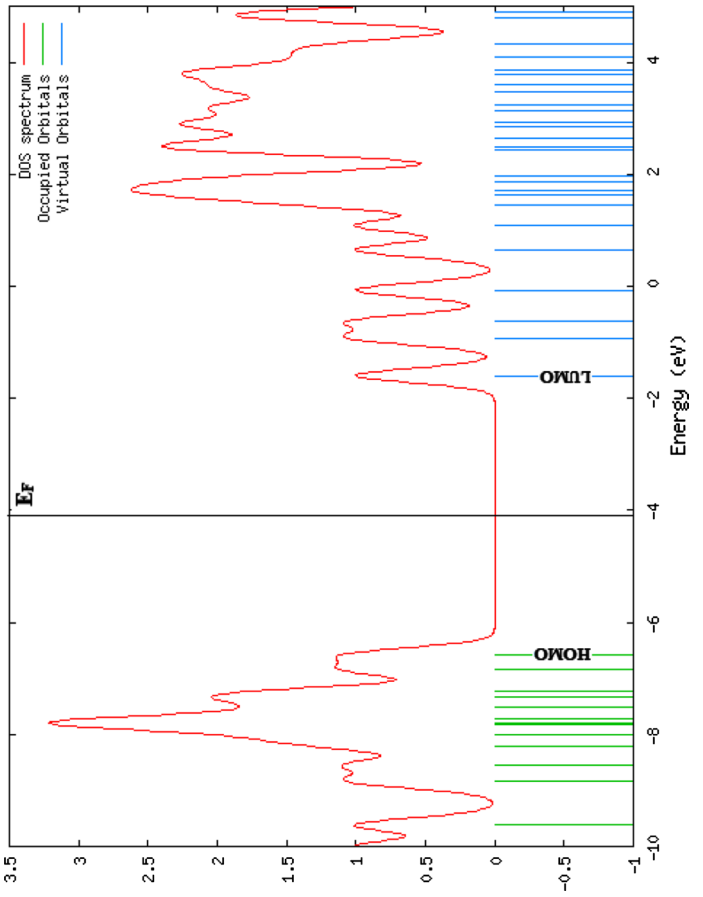

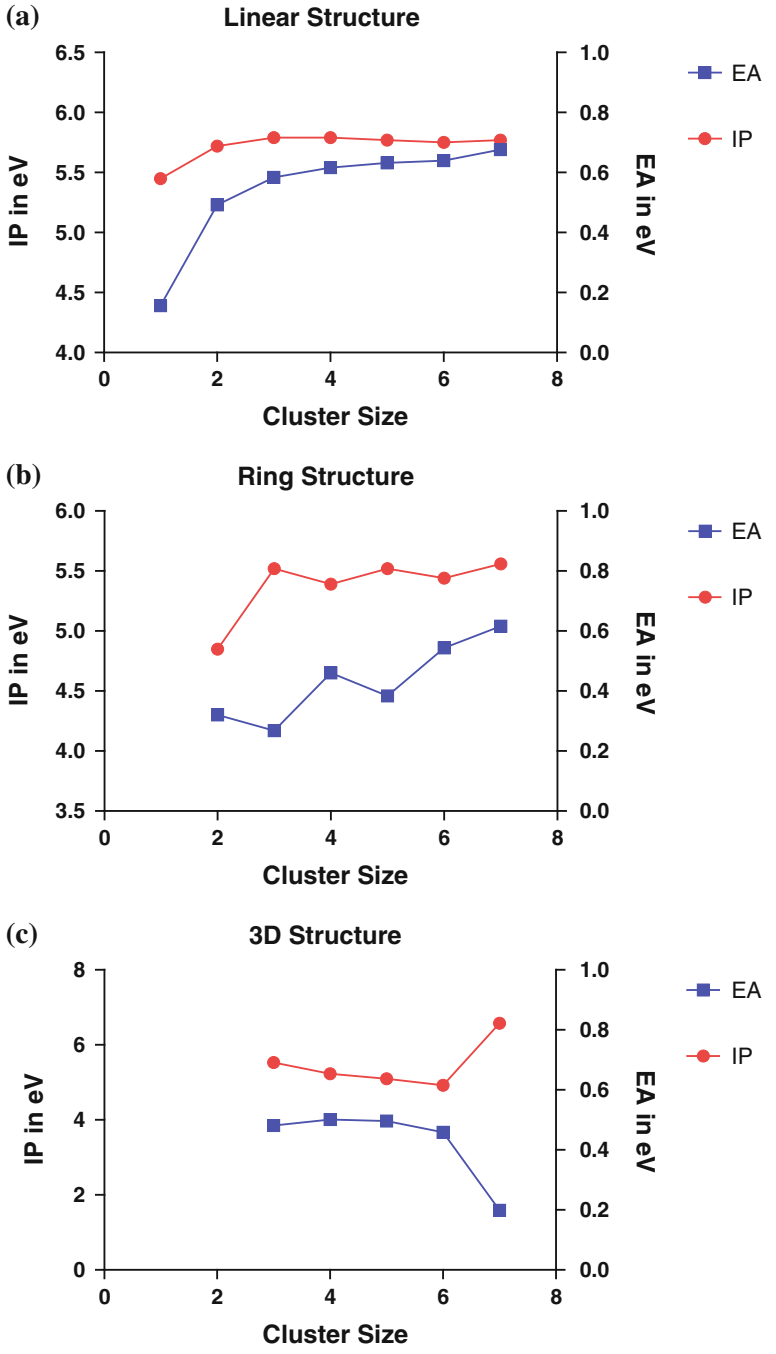

Fig. 4 **a** Variation of IP and EA with cluster size for $(CdTe)_n$ ($n = 2$–7) linear clusters **b** Variation of IP and EA with cluster size for $(CdTe)_n$ $n = 2$–7 ring clusters **c** Variation of IP and EA with cluster size for $(CdTe)_n$ for $n = 2$–7 3D clusters

$$\Delta_2(n) = \left\{E\left[(\mathrm{CdTe})_{n+1}\right] + E\left[(\mathrm{CdTe})_{n-1}\right] - 2E\left[(\mathrm{CdTe})_n\right]\right\}$$

where n represents cluster size [33]. In Fig. 5 the dependence of calculated relative stability on cluster size is plotted for the three different CdTe structures. For the linear structure we notice an increase in stability when cluster size increases, which implies addition of more atoms increases its stability; because the structure is truncated at both ends, stability is less for all the linear structures than for the other two structures. For the ring structures of CdTe with $n = 3$ and 5 stability is low whereas for $n = 6$ the stability is high because of the positions of the atom in this ring structure. There is an increasing trend in the stability of the 3D structure, because of its cube like structure. For 3D clusters with higher values of n the stability increases steadily, because of the uniformity of atom arrangement in the cluster.

Binding energies of $(\mathrm{CdTe})_n$ clusters

The binding energy per atom (BE) is calculated by use of the equation:

$$\mathrm{BE} = (n \times E[\mathrm{Cd}] + n \times E[\mathrm{Te}] - E\left[(\mathrm{CdTe})_n\right])/(n)$$

where E[Cd] is the energy of the cadmium atom, E[Te] is the energy of tellurium atom and n is the number of atoms in the clusters [34, 35]. The binding energies of $(\mathrm{CdTe})_n$ for $n = 2$–7 clusters are listed in Table 4. The binding energy of linear structure seems to increase with cluster size, which is in agreement with the energy calculated in Hartrees. This implies that the stability of the linear structure increases with increasing number of atoms. For the ring structure the BE has zigzag variation, because of the formation of the closed loop. The closed loop in these structures will give rise to overlap of orbitals, resulting in complex variation in BE. The 3D structures have higher values than the linear and ring structures, because the regular arrangement of atoms in these structures results in increased stability. Calculated BE is in good agreement with reported BE for CdTe nanoclusters [36].

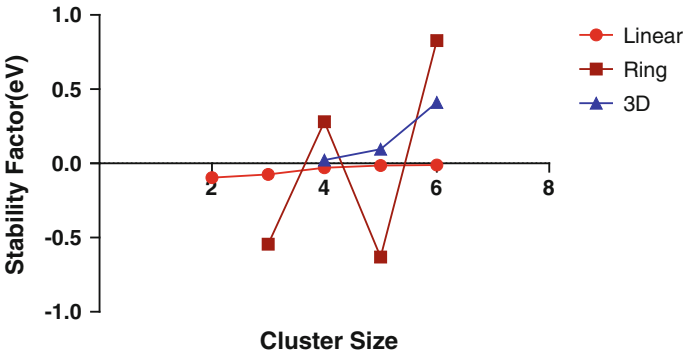

Fig. 5 Variation of stability with cluster size for the three different structures of $(\mathrm{CdTe})_n$ ($n = 2$–7)

Table 4 Binding energies of $(CdTe)_n$ ($n = 2$–7) clusters

Structure	Cluster size	Binding energy (eV)
Linear	1	0.802
	2	1.04
	3	1.183
	4	1.251
	5	1.289
	6	1.312
	7	1.325
Ring	2	1.204
	3	1.605
	4	1.462
	5	1.600
	6	1.106
	7	1.44
3D	3	1.546
	4	1.53
	5	1.537
	6	1.639
	7	2.152

Conclusion

Using DFT approach with the B3LYP/LanL2DZ basis set, linear, ring, and 3D clusters of $(CdTe)_n$ ($n = 2$–7) were completely optimized. Addition of atoms to the clusters increased their stability. The energy difference between two successive clusters was 56 Hartrees. There was no significant variation in the energy of ring and 3D structures. Variation is seen in the fractional part, only, among linear, ring, and 3D structures. Ring structures have lower dipole moments than linear and 3D structures. The clusters can be in any of the point groups $C_{\infty V}$, C_1, C_S, or C_{2V}. The HOMO–LUMO gaps of the linear structures are almost identical, whereas for the ring structure the gap increases or decreases depending on the position of the atoms in the cluster. The HOMO–LUMO gap is substantial for the 3D structure. There is no drastic variation of ionization potential among the linear structures. The ionization potential for the ring structures follows a zigzag path. The ionization potentials of 3D structures are almost identical. The electron affinity varies randomly with cluster size. Increasing stability of the 3D structure is because of uniform packing of the atoms. Interestingly, the 3D structures have higher binding energy than the linear and ring structures, again because of the regular arrangement of their atoms. Determination of the properties of different clusters of $(CdTe)_n$ ($n = 2$–7) may aid future synthesis of CdTe nanoclusters of potential importance in the fabrication of solar cells.

References

1. K. Omura, A. Hanahusa, T. Arita, H. Higuchi, T. Aramoto, T. Nishio, S.Sibutani, S. Kumazawa, M. Murozono,in *WREC*, (1996), p.405
2. X. Wu, Sol. Energy **77**, 803 (2004)
3. C.S. Ferekides, U. Balasubramanian, R. Mamazza, V. Viswanathan, H. Zhao, D.L. Morel, Sol. Energy **77**, 823 (2004)
4. O. Mahammad Hussain, P. Jayarama Reddy, J. Mater. Sci. Lett. **10**, 813 (1991)
5. G.S. Khrypunov, E.P. Chernykh, N.A. Kovtun, E.K. Belonogov, Semiconductors **43**, 1046 (2009)
6. D.C. Harris, Infrared Phys. Technol. **39**, 185 (1998)
7. J. Rutkowski, P. Madejczyk, A. Piotrowski, W. Gawron, K. JóWikowski, A. Rogalski, Opto-Electron. Rev. **16**, 321 (2008)
8. J.P. Zanatta, P. Ferret, G. Theret, A. Million, M. Wolny, J.P. Chamonal, G. Destefanis, J. Electron. Mater. **27**, 542 (1998)
9. L. Verger, J.P. Bonnefoy, F. Glasser, P. Ouvrier-buffet, J. Electron. Mater. **26**, 738 (1997)
10. S.S. Yoo, G. Jennings, P.A. Montano, J. Electron. Mater. **26**, 750 (1997)
11. A. Milani, E. Bocchi, A. Zappettini, S.M. Pietralunga, M. Martinelli, J. Cryst. Growth **214/215**, 913 (2000)
12. P.C. Sarmah, A. Rahman, Bull. Mater. Sci. **21**, 149 (1998)
13. S.V. Krishnaswamy, R. Messier, P. Swab, L.L. Tongson, K. Vedam, J. Electron. Mater. **10**, 433 (1981)
14. L.A. Kosyachenko, X. Mathew, V.V. Motushchuk, V.M. Sklyarchuk, Sol. Energy **80**, 148 (2006)
15. M.N. Mamedov, A.Sh. Aliev, Inorg. Mater. **44**, 804 (2008)
16. A.K. Berry, Mater. Sci. Eng. B **8**, 57 (1991)
17. R. Diamant, L. Ponce, M. Fernez, E. Jimenez, Appl. Phys. B **66**, 639 (1998)
18. A.S. Yeremyan, H.N. Avetisyan, L.G. Arshakyan, Pulsed Laser Deposition of Layers and Nanostructures Based on CdTe and Bi. NATO Sci peace and secur. series B: phys. biophys. **2009**, 307–312 (2009)
19. K. Kim, K. Kim, H.J. Kim, S.-H. Suh, M. Carmody, S. Sivananthan, J.-S. Kim, J. Electron. Mater. **39**, 863 (2010)
20. Z. Wu, Z. Yonghong, H. Shiping, Shengli. Zhang, Comput. Mater. Sci. **68**, 238 (2013)
21. M. Li, W. Jianguang, W. Guanghou, Chem. Phys. Lett. **552**, 73 (2012)
22. N.A. Noor, S. Ali, A. Shaukat, J. Phys. Chem. Solids **72**, 836 (2011)
23. M.J. Frisch, G.W. Trucks, H.B. Schlegel, G.E. Scuseria, M.A. Robb, J.R. Cheeseman, V.G. Zakrzewski, J.A. Montgomery Jr, R.E. Stratmann, J.C. Burant, S. Dapprich, J.M. Millam, A.D. Daniels, K.N. Kudin, M.C. Strain, O. Farkas, J. Tomasi, V. Barone, M. Cossi, R. Cammi, B. Mennucci, C. Pomelli, C. Adamo, S. Clifford, J. Ochterski, G.A. Petersson, P.Y. Ayala, Q. Cui, K. Morokuma, D.K. Malick, A.D. Rabuck, K. Raghavachari, J.B. Foresman, J. Cioslowski, J.V. Ortiz, A.G. Baboul, B.B. Stefanov, G. Liu, A. Liashenko, P. Piskorz, I. Komaromi, R. Gomperts, R.L. Martin, D.J. Fox, T. Keith, M.A. Al-Laham, C.Y. Peng, A. Nanayakkara, C. Gonzalez, M. Challacombe, P.M.W. Gill, B.G. Johnson, W. Chen, M.W. Wong, J.L. Andres, M. Head-Gordon, E.S. Replogle, J.A. Pople, *Gaussian 99* (Gaussian Inc, Pittsburgh, 1998)
24. R. Srinivasaraghavan, R. Chandiramouli, B.G. Jeyaprakash, S. Seshadri, Spectrochim. Acta, Part A. Mol. Biomol. Spectrosc. **102**, 242 (2013)
25. T.A. Yu, Russ. J. Inorg. Chem. **54**, 86 (2009)
26. V.I. Minkin, R.M. Minyaev, A.A. Milov, T.N. Gribanova, Russ. Chem. Bull. **50**, 2028 (2001)
27. M. Monajjemi, M.T. Baei, F. Mollaamin, Russ. J. Inorg. Chem. **53**, 1430 (2008)
28. N.M. O'Boyle, A.L. Tenderholt, K.M. Langner, J. Comp. Chem. **29**, 839 (2008)
29. R. John Xavier, E. Gobinath, Spectrochim. Acta, Part A **97**, 215 (2012)
30. M. Arivazhagan, S. Jeyavijayan, Spectrochim. Acta Part A **79**, 376 (2011)
31. S.K. Bhattacharya, A. Kshirsagar, Eur. Phys. J. D **61**, 609 (2011)
32. C.-G. Zhan, J.A. Nichols, D.A. Dixon, J. Phys. Chem. A **107**, 4184 (2003)
33. A. Dwivedi, N. Misra, J. At. Mol. Sci. **3**(2012), 285–296 (2012)
34. D. Bandyopadhyay, J. Mol. Model. **18**, 737 (2012)
35. N. Misra, A. Dwivedi, A.K. Pandey, J. At. Mol. Sci. **3**, 187 (2012)
36. S.K. Bhattacharya, A. Kshirsagar, Phys. Rev. B **75**, 035402 (2007)